Solar Energy 147 (2017) 381–389

Contents lists available at ScienceDirect

Solar Energy

journal homepage: www.elsevier.com/locate/solener

Enhancing energy harvest in a constructal solar collector by using alumina-water as nanofluid

J.A. Ojeda [a,*], S. Messina [b]

[a] Facultad de Arquitectura y Diseño, Universidad de Colima, Km. 9-Colima-Coquimatlán Driveway, 28400 Coquimatlán, Colima, Mexico
[b] Unidad de Ciencias Básicas e Ingeniería, Universidad Autónoma de Nayarit, Cd. de la Cultura Amado Nervo S/N, 63155 Tepic, Nayarit, Mexico

ARTICLE INFO

Article history:
Received 29 September 2016
Received in revised form 2 March 2017
Accepted 18 March 2017
Available online 27 March 2017

Keywords:
Nanofluid
Constructal design
Solar energy
Solar collector

ABSTRACT

We have developed a network of pipes of dendritic geometry in a solar collector with a disc-shaped body. The fluid in the network pipes is a nanofluid composed of a mixture of nanoparticles of alumina (Al_2O_3) and water as a base fluid in order to harvest a greater amount of thermal energy from incoming solar radiation. The sizes of the network pipes are obtained by using constructal theory methods. Thermal conductivity was obtained by the Hamilton-Crosser model; physical properties such as density and specific heat capacity were described as a function of the volumetric fraction of nanoparticles in the fluid. Optimal size of the network presented for every level of construction was established by the condition of minimal thermal resistance. Temperature profiles and the aspect ratio of the construction elements were defined as a function of the volumetric fraction of nanoparticles. Results show that by increasing the volume fraction of nanoparticles, thermal energy gain also increases, reaching a higher outlet temperature of the fluid when alumina nanoparticles are used.

1. Introduction

The increase in world energy demand and the progressive depletion of fossil fuels necessitate the development of technologies based on alternative energy sources. Solar energy is widely used for heating water for domestic and industrial purposes through solar collectors (Kalogirou, 2004). Solar collectors are classified as low temperature devices with operation ranges of 20–150 °C. The flat-plate solar collector is the most widely used. The working fluid flowing in the pipe network is generally water. It is possible nowadays to use, as a working fluid a colloidal suspension with nano-sized solid particles (1–100 nm). Such suspensions are composed of metal particles (oxides) dispersed uniformly, and a base fluid. This combination can present higher thermo-physical properties, such as thermal conductivity values superior to conventional working fluids like water; these particular features are used to improve heat transfer processes (Puliti et al., 2012).

The modification of the thermal properties of a colloidal suspension is possible by adding nano-sized metal particles in a base fluid. The resulting fluid is known as a nanofluid (Buongiorno et al., 2009; Keblinski et al., 2005). The increase of thermal conductivity is due to physical factors such as the Brownian movement of particles in the fluid, a liquid layer at the liquid-particle interface, nanoparticle clustering and concentration of the nanoparticle in the base fluid (Angayarkanni and Philip, 2015; Keblinski et al., 2002). Theoretical and experimental work on the thermal and rheological properties of nanofluids, for different particle materials, is reported mainly in fluid mixtures with oxide particles in convective heat transfer processes (Buongiorno, 2006; Daungthongsuk and Wongwises, 2007; Ghanbarpour et al., 2014). The particular thermal properties of these fluids represent an option for the design of cooling systems in electronic, aerospace and automotive industries through the design of microchannel devices (Chen and Ding, 2011; Khaleduzzaman et al., 2014; Koo and Kleinstreuer, 2005), in designing techniques of drug delivery in the human body (Abbasi et al., 2015; Kleinstreuer et al., 2008), heating, ventilation and air conditioning systems (Hatami et al., 2017), refrigeration systems (Sözen et al., 2014) and optical filters for thermo-photovoltaic solar systems (Taylor et al., 2012). A numerical study for a solar collector with a nanofluid as a working fluid is reported by Nasrin and Alim (2014), identifying the influence of the characteristic dimensionless numbers of the problem as a factor to improve the efficiency collector. Experimental nanofluid applications in conventional flat-plate solar collectors are reported widely by Sarsam et al. (2015), where the main topic is the improved efficiency and performance.

* Corresponding author.
E-mail address: jojeda1@ucol.mx (J.A. Ojeda).

http://dx.doi.org/10.1016/j.solener.2017.03.054
0038-092X/

Nomenclature

A	area of the semi-circular sector (m^2)
C	specific heat capacity (J/kg K)
D	diameter (m)
H	height of the constructal element (m)
k	thermal conductivity
L	length of the constructal element (m)
R	radius (m)
t	physical time (seg)
V	volume of the constructal element (m^3)
w	width of the constructal element (m)
$\dot{q}$	heat flux (W/m^2)

Greek symbols

ω	frequency of the solar signal (1/seg)
ϕ	volumetric fraction of the particle
ρ	density (kg/m^3)

Subscripts

p	particle
f	fluid
nf	nanofluid
0	refers to the first construction
1	refers to the first level ramification
2	refers to the second level of ramification

Applications of nanofluids in thermal systems are reported mainly to improve the performance of the heating systems. Lu et al. (2011) conducted an experiment of an open thermosyphon applied in an evacuated tubular solar heating system with an evaporator tube and two working fluids, deionised water and a water-based copper oxide nanofluid in order to evaluate the thermal performance of the system under steady operative conditions, such as pressure and temperature under indoor conditions. The point of operation of heat transfer enhancement of the system was found for a specific value of the mass concentration of the nanoparticles.

The heating system mentioned previously established the experimental conditions for an outdoor experiment applied to a simplified compound solar concentrator as a solar air collector with the same working fluids. The main results are efficiency improvement with a nanofluid with the mass concentration determined previously (Liu et al., 2013). These works provide important information about the experimental procedures in collector systems and demonstrate the existence of an optimal point of operation for a thermal system for a specific value of the concentration of nanoparticles in a fluid base.

The design of nanofluids with suitable thermo-physical properties (high thermal conductivity) will allow the design of efficient systems for heat removal, miniaturisation of the devices and the consequent energy savings (Godson et al., 2010).

The constructal theory, proposed by Bejan (2000), develops transport networks to imposed physical flows (heat, fluid) with the principal characteristic of obtaining a minimal resistance to flow, under local restrictions, that satisfy a main objective. The design methodology allows networks with different geometrical configurations (shape and structure) to have optimal transportation between a point and an infinite number of points, area or volume.

In an effort to apply the constructal theory to designing nanofluids, Fan and Wang (2010) report the microstructure of a single nanoparticle immersed in the base fluid, which is defined by the minimal thermal resistance. The elemental system is a nanoparticle with a source of uniform heat in a disc-shaped element; the particle is defined as plates of slabs of a thermal conductivity value, higher than the base fluid. The system optimisation is determined by the freedom within the three-shaped nanostructures.

On the other hand, Bai and Wang (2011) developed the expressions for the thermal resistance of constructal building blocks composed of a base fluid and nanoparticles with blade configuration. The constructal theory is applied to describe the optimal shape for the blades, cylinder-shape and prism-shape of the particle, that offers minimum thermal resistance. Both studies focus on the design of the microstructure of the nanoparticle from the principles of optimisation of the constructal theory. The same group developed the design of the microstructure of a nanofluid by comparing two geometric configurations—quasi-rhombus and quasi-sector shapes—identifying a proper nanofluid configuration for better heat transfer performance (Bai and Wang, 2013). An important parameter for increasing the thermal conductivity of a nanofluid is the geometry of the particle. This aspect is considered as a shape factor in theoretical models.

In the present work we develop a pipe network with a dichotomous branching characteristics following the constructal methods by treating the nanofluid as a medium that flows to remove heat in a disc-shaped body system. The nanofluid properties such as thermal conductivity, density and specific heat capacity are modelled as a function of the physical properties of the alumina nanoparticle, water as a base fluid and volumetric fraction.

2. First element or construction

The first element of construction takes into account the physical and geometrical variables and considers the finite size volume that is initially found at a uniform temperature T_0. This element is a semi-circular sector with area A_0 and volume V as constants, which are local constraints. These assumptions are the restrictions that are frequently assumed by the constructal theory. The solar incident area is given by $A_0 \approx H_0 L_0$, where the height and length of the disc-shaped body are unknown and determined from the optimisation process.

The constructal theory considers the total volume of the pipe network system as a building block of elements, optimised in shape and form; the optimisation process begins with the first element of construction (Wechsatol et al., 2002). Fig. 1 provides a sketch and the dimensions of this first element.

The top of the element is separated by an infinitesimal wall with negligible thermal conductivity. In the transverse direction, at $y = H_0$, the element receives the solar energy; the limits of the constructal element are at temperature T_m. For simplicity, we consider that the warming effect of air trapped in the cavity comes from the signal $\dot{q} = \dot{q}_0 sin(\omega t)$, where $\dot{q}_0$ is the reference amplitude of this periodic heat flux for the present system, ω is the frequency of the solar signal and t is the physical time. The space between the surface exposed to solar radiation and the pipe of diameter D_0 is considered a cavity filled with air at temperature T_c.

Inside the pipe, a nanofluid is circulating in the x direction in a steady-state regime. This hypothesis is justified below. The nanofluid flow is considered Newtonian and fully developed, and is considered to be stable (no chemical reactions) with nanoparticles of

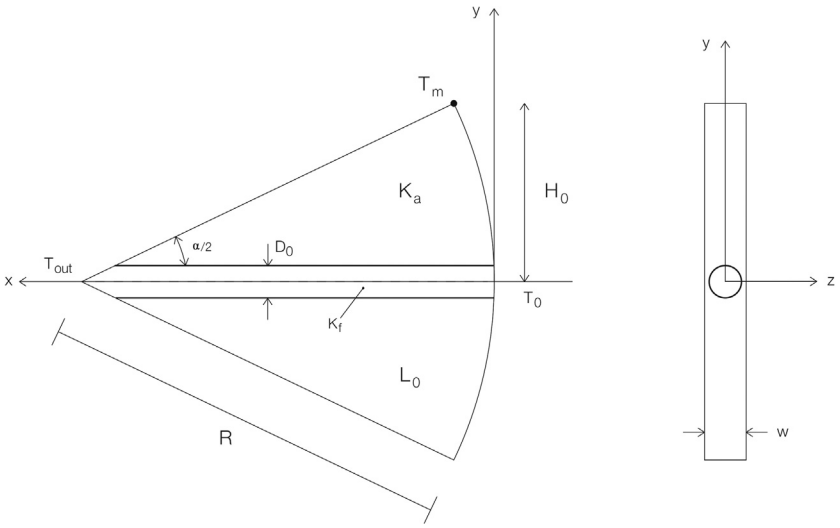

Fig. 1. First element of construction.

uniform size and in thermal equilibrium. The value of viscosity of the nanofluid is assumed as constant and equal to the base fluid.

The fluid flows from the periphery to the centre of the semicircular sector. The nanofluid enters at temperature T_0 and leaves the element at a higher temperature T_{out} due to the heating process. The last temperature is unknown and must be determined as part of the problem, together with the lengths H_0 and L_0. The angle α of the circular sector is given by $\alpha = 2\pi/n_0$, where n_0 is the number of pipes of diameter D_0 that transports a fluid to the centre of the constructal element; for the case of a Newtonian fluid with the minimum flow resistance, the minimum number of pipes is $n_0 = 3$ (Wechsatol et al., 2002).

In order to describe the thermal conductivity of the nanofluid, we propose a variant of the Maxwell model, known as the Hamilton-Crosser model (Hamilton and Crosser, 1962), which is a function of the thermal conductivities of the particle, base fluid, volumetric fraction and shape factor n. For a spherical particle it presents a value of $n = 3$; for a cylindrical particle the shape factor is $n = 6$. The model mentioned above is given by Eq. (1):

$$k_{nf} = \frac{k_p + (n-1) - (n-1)(k_p - k_f)\phi}{k_p + (n-1)k_f + (k_p - k_f)\phi} k_f, \tag{1}$$

where k_p, k_f are the thermal conductivities of the particle and the base fluid, respectively, and ϕ is the volumetric fraction of the nanoparticles.

The density and specific heat capacity of the nanofluid are defined as a function of the volumetric fraction, properties of the particle and the base fluid (Drew and Passman, 1999). The expressions of the previously mentioned properties are defined as

$$\rho_{nf} = \phi\rho_p + (1-\phi)\rho_f; \tag{2}$$

$$(\rho C_P)_{nf} = (\rho C_p)_p \phi + (1-\phi)(\rho C_p)_f. \tag{3}$$

Properties of the alumina (Al_2O_3) and water as a base fluid are assumed as constants; the values are widely reported by Büyük Öğüt (2009). For a volumetric fraction less than or equal to 0.04, the nanofluid is categorised as semidiluted (Puliti et al., 2012). For this value of volumetric fraction, the mixture alumina water presents Newtonian behaviour (Putra et al., 2003). From Eqs. (1)–(3), for a null value of the volumetric fraction ($\phi = 0.0$) the base fluid properties are obtained.

3. Mathematical model

Optimisation of the first constructal element begins with a definition of the temperature profiles, in the vertical (air) and horizontal (fluid) directions. It is known that in a cavity filled with air, the heat transfer processes in a slender cavity are governed only by accumulation and diffusive terms of the energy equation because the convective terms are of the order of the Rayleigh number (Bejan, 2013). In the slender cavity of the first element, we assume that $H_0 \ll L_0$. With this scale we consider, as a first approximation, that the heat transfer is dominated only by a conductive heat transfer regime with the objective of applying the constructal methods. The characteristic time scale is given by $1/\omega$ [s] and is defined by comparing the residence time of the fluid in the pipe of diameter D_0 and the inverse of the frequency of the sinusoidal solar signal described above.

From an energy balance we can define the differential partial equation in the cavity filled with air:

$$\sin(\omega t) + \frac{k_{air} w}{\dot{q}_0} \frac{\partial^2 T_c}{\partial y^2} = \frac{\rho C_P w}{\dot{q}_0} \frac{\partial T_c}{\partial t}. \tag{4}$$

The following dimensionless variables are used to simplify the number of physical parameters involved:

$$\chi = \frac{x}{L_0}, \eta = \frac{y}{H_0}, \theta_c = \frac{T_c - T_0}{\Delta T}, \theta_f = \frac{T_f - T_0}{\Delta T} \tau = \omega t, \tag{5}$$

where $\Delta T = T_m - T_0$. Then, Eq. (5) can be rewritten as,

$$\sin(\tau) + \alpha \frac{\partial^2 \theta_c}{\partial \eta^2} = \beta \frac{\partial \theta_c}{\partial \tau}, \tag{6}$$

where $\beta = \rho C_P \Delta T w \omega / \dot{q}_0 \sim 10^{-6}$, and therefore, the energy accumulation term can be neglected. Thus, a quasi-stationary state is assumed. The boundary conditions to solve Eq. (5) are the following;

$$\eta = 0 : \theta_c = \theta_f(\chi = 1); \eta = 1; \frac{\partial \theta_c}{\partial \eta} = 0. \tag{7}$$

The solution of the Eq. (6), subject to boundary conditions, can be obtained and is given by:

$$\theta_c(\eta) = \frac{\sin(\tau)}{\alpha}\left(\eta - \frac{\eta^2}{2}\right) + \theta_f(\chi = 1). \tag{8}$$

Similarly, we can carry out an energy balance in the pipe region, taking accumulative, conductive, convective and radiative energy terms into account, resulting in dimensionless units in the following partial equation:

$$\frac{\alpha_{nf}}{Pe}\varepsilon_0\frac{\partial^2\theta_f}{\partial\chi^2}-\frac{4}{3}\frac{\partial\theta_f}{\partial\chi}+\epsilon\frac{\partial\theta_f}{\partial\tau}+\frac{4\alpha_{nf}\gamma_0}{Pe}sin(\tau)=0, \tag{9}$$

where $\epsilon=\omega L_0/U_{prom}\sim 10^{-8}$, and the accumulation term can be neglected. Thus, a quasi-stationary state is assumed for the circulating nanofluid, and the dimensionless parameters in Eq. (9) are defined as follows: $\varepsilon_0=D_0/L_0$, $\gamma_0=\dot{q}_0L_0/\Delta Tk_{nf}$, $Pe=U_{av}D_0/\alpha_f$, where Pe represents the Peclet number defined with an average velocity U_{av}, related to the characteristic velocity of the fluid and the pressure gradient.

Eq. (9) takes into account that the transverse temperature variations are smaller than the horizontal temperature variations. As a first approximation, the temperature of the fluid is a function only of the longitudinal coordinate x; that is, $T\cong T(x)$. This is a thin-fin approximation used in constructal theory procedures for modelling heat transfer thermal cases (Bejan, 2000). In addition, in Eq. (9) we consider that for the infinitesimal surface that separates the cavity from the fluid trapped in the pipe, the boundary condition $h(T_{sur}-T_0)=-k_a(\partial T_a/\partial y)|_{y=R_0}$ is fulfilled. This allows the heat transfer process between the cavity and the nanofluid as a first approximation to implement the constructal optimisation methods to design pipe networks. This formulation enables us to interpret the radiative signal as a warming effect of air trapped in the cavity from the signal $\dot{q}=\dot{q}_0sin(\omega t)$, which is an approximation of the radiation energy.

The boundary conditions to solve Eq. (9) are the following:

$$\chi=0:\theta_f=0;\chi=1;\frac{\partial\theta_f}{\partial\chi}=0. \tag{10}$$

The solution to Eq. (9) subject to the boundary conditions, Eq. (10), can be obtained and is given by:

$$\theta_f(\chi)=\frac{9}{4}\sin(\tau)\frac{\gamma_0\varepsilon_0\alpha_{nf}^2}{Pe^2}exp\left(-\frac{4}{3}\frac{Pe}{\varepsilon_0\alpha_{nf}}\right)\left(1-exp\left(\frac{4}{3}\frac{Pe}{\varepsilon_0\alpha_{nf}}\chi\right)\right)+\frac{3\gamma_0\alpha_{nf}}{Pe}\sin(\tau)\chi, \tag{11}$$

where α_{nf} is the thermal diffusivity as a function of the volumetric fraction ϕ, defined with Eqs. (1)–(3).

The temperature profile in the longitudinal coordinate, for high values of the Peclet number, $Pe\gg 1$, the first term of Eq. (11) tends to be zero; thus we can approximate the temperature profile to a linear behaviour, as follows:

$$\theta_f(\chi)\approx 3\gamma_0\alpha_{nf}\sin(\tau)\chi/Pe. \tag{12}$$

The simplification of the temperature profile in direction x more easily defines the temperature differences in the first constructal element and the average Nusselt number evaluated along the longitudinal direction. The heat transfer process between the wall of the pipe and the fluid is considered by the average Nusselt number based on the assumption that the convective heat transfer coefficient is a function of longitudinal coordinate $h(x)$.

The wall temperature θ_w, is calculated by the Eq. (8) at $\eta=\varphi_0$, $(y=R_0)$; the heat transferred from the cavity to the fluid is defined as $\dot{q}=\dot{q}_0\sin(\omega t)=h(x)(T_w-T(x))$. On the other hand, the Nusselt number is defined as $Nu=h(x)x/k_{nf}$, such that with the aid of the Eq. (13), we can define an expression of the average Nusselt number, evaluated along the longitudinal axis of the pipe. This expression, in dimensionless variables, is given by:

$$Nu_{av}=\frac{Pe^2}{9\gamma_0\alpha_{nf}^2}\left[\frac{1}{\alpha}\left(\varphi_0-\frac{\varphi_0^2}{2}\right)+3\frac{\alpha_{nf}\gamma_0}{Pe}\right]ln\left\{1+\frac{6\alpha_{nf}\gamma_0\alpha}{Pe(2\varphi_0-\varphi_0^2)}\right\}-\frac{Pe}{3\alpha_{nf}} \tag{13}$$

where $\varphi_0=R_0/H_0$ is a geometrical parameter.

The temperature difference of the first element of construction is defined in a vertical and horizontal direction with the aid of the Eqs. (8) and (12)–(14). The first temperature difference is in the case of the cavity filled with air, evaluating from the farthest point from the pipe, at $\eta=1(y=H_0)$ and the wall temperature at $\eta=\varphi_0(y=R_0)$; the second temperature difference is defined by the temperature of the fluid at the inlet of the pipe at $\chi=0,(x=0)$ and at the temperature at the outlet $\chi=1,(x=L_0)$. The third temperature difference is defined with the aid of the Eqs. (12) and (13); the expressions defining the total temperature difference in the constructal element are given by;

$$\theta_m-\theta_w=\frac{\sin(\tau)}{\alpha}\left[\frac{1}{2}(1+\varphi_0^2)-\varphi_0\right], \tag{14}$$

$$\theta_{f-out}-\theta_{f-in}\approx\frac{3\gamma_0\alpha_{nf}\sin(\tau)}{Pe}, \tag{15}$$

$$\theta_w-\theta_{f-out}=\frac{\gamma_0\sin(\tau)}{Nu_{av}}. \tag{16}$$

The methodology to define the thermal resistance in constructal elements is widely documented by Wechsatol et al. (2002), for the case of a semi-circular sector with a radial pipe, where a nanofluid flows from the periphery to the centre and is defined as $\widetilde{T}_0=(\theta_m-\theta_{f-in})k_{air}\Delta T/\dot{q}_0A_0^{1/2}$. From algebraic simplifications we can define, with the aid of the Eqs. (14)–(16), an expression for the thermal resistance of the first element, given by;

$$\widetilde{T}_0=\left[\Pi_0\widehat{H}_0\left(\frac{1}{2}(1+\varphi_0^2)-\varphi_0\right)+\frac{3\kappa\alpha_{nf}}{\widehat{H}_0Pe}+\frac{\kappa}{\widehat{H}_0Nu_{av}}\right]\sin(\tau), \tag{17}$$

where $\Pi_0=H_0/w$, $\widehat{H}_0=(H_0/L_0)^{1/2}$, are geometrical parameters. In addition, $\kappa=k_{air}/k_{nf}$; the thermal conductivity of the nanofluid, k_{nf} is defined by the Hamilton-Crosser model.

Eq. (18), defines the thermal resistance of the first element of construction. This equation is a function of the aspect ratio $\widehat{H}_0$ and represents the size of the element. From the initial assumption, the geometry of the first element is slender and it is expected that the value of the aspect ratio will be small. We anticipated that the aspect ratios for every level of construction of the pipe network would be small, as shown in the results section. The expression for the thermal resistance presents a minimum, and is shown below:

$$\widehat{H}_0=\left[\frac{\frac{3\kappa\alpha_{nf}}{Pe}+\frac{\kappa}{Nu_{av}}}{\Pi_0\left(\frac{1}{2}(1+\varphi_0^2)-\varphi_0\right)}\right]^{\frac{1}{2}}. \tag{18}$$

4. Second and third construction

A branched network is generated inside the solar collector of a disc-shaped body of radius R, and a second construction is defined as two semi-circular slender building blocks, with pipes of diameter D_1, which connects with the pipe of diameter D_0 of the first constructal element, this is designate as a first level of ramification. The dichotomy of tubes is a characteristic of the network of pipes and the flow architecture is a result of the constructal methods of optimisation. The bifurcation of pipes in every level of ramification makes the connection of many points in the periphery to one point

in the path of least flow resistance (Bejan, 2000). In the method of constructal theory to design networks, the Hess-Murray law has been demonstrated; to minimising the flow resistance in a branched (dichotomy) network with a Newtonian fluid, the mentioned law is given by $D_i/D_{i+1} = 2^{1/3}$, where i is the ramification level (Miguel, 2015). A flow structure with dichotomy characteristics is assumed in every level of ramification. In this work we applied this law to the second and third construction.

In the second element of construction, the restrictions of area and volume are applied. According to the constructal method, the lengths H_1 and L_1 are unknown. The process of optimisation applied in the first constructal element is recursive to successive branches. Fig. 2 provides a sketch and the dimensions of this second element of construction.

The temperature profiles for the ramified pipe of the second construction are obtained with the methodology applied in the previous section. In order to describe the temperature increase due to the solar collection with a branched network, we consider that the outlet fluid temperature of the pipe of diameter D_1 is the same for the inlet fluid temperature in the pipe of diameter D_0. This is considered in the respective boundary conditions of the differential equation for the fluid temperature profile of the pipe of diameter D_0. The fluid flows from the periphery to the centre of the semi-circular sector along the branched pipes. In the geometrical arrangement of a Y-shape with two L_1 pipes and one L_0 pipe, the lengths can be defined as a function of radius of the disc-shaped body R and the angle of bifurcation β; the lengths are easily defined as:

$$L_0 = R\cos\left(\frac{\alpha}{4}\right) - L_1\cos(\beta); L_1 = R\frac{\sin\left(\frac{\alpha}{4}\right)}{\sin(\beta)}. \tag{19}$$

Optimal lengths are defined, minimising the pressure drop between the periphery and the centre, with a constant volume of the arrangement of pipes as a restriction. The Hess-Murray law is considered in the previous restriction. Angle α is known and defined by n_0, defined in the first constructal element. The calculated angle β, which has a minimum flow resistance, is $\beta = 37.46^\circ$ (Wechsatol et al., 2002).

These lengths are considered in the longitudinal temperature profiles of the first and second constructal elements; consequently, the average Nusselt number, thermal resistance and aspect ratio can be obtained by applying the method described in the previous section. The thermal resistance of the second constructal element is defined by the following expression:

$$\widetilde{T}_1 = \left[\Pi_1\widehat{H}_1\left(\frac{1}{2}(1+\varphi_1^2) - \varphi_1\right) + 2^{\frac{1}{3}}\frac{3\kappa\alpha_{nf}}{\widehat{H}_1 Pe} + \frac{\kappa}{\widehat{H}_1 Nu_{av1}}\right]\sin(\tau). \tag{20}$$

Therefore, the aspect ratio of the second constructal element, $\widehat{H}_1$ is given by;

$$\widehat{H}_1 = \left[\frac{\frac{3\kappa\alpha_{nf}}{Pe} + \frac{\kappa}{Nu_{av1}}}{\Pi_1\left(\frac{1}{2}(1+\varphi_1^2) - \varphi_1\right)}\right]^{\frac{1}{2}} \tag{21}$$

On the other hand, for a third constructal element the geometrical arrangement of pipes consists of four pipes of diameter D_2 and length L_2, two pipes with diameter and length D_1, L_1 and one pipe of diameter and length D_0, L_0. The optimisation process is applied

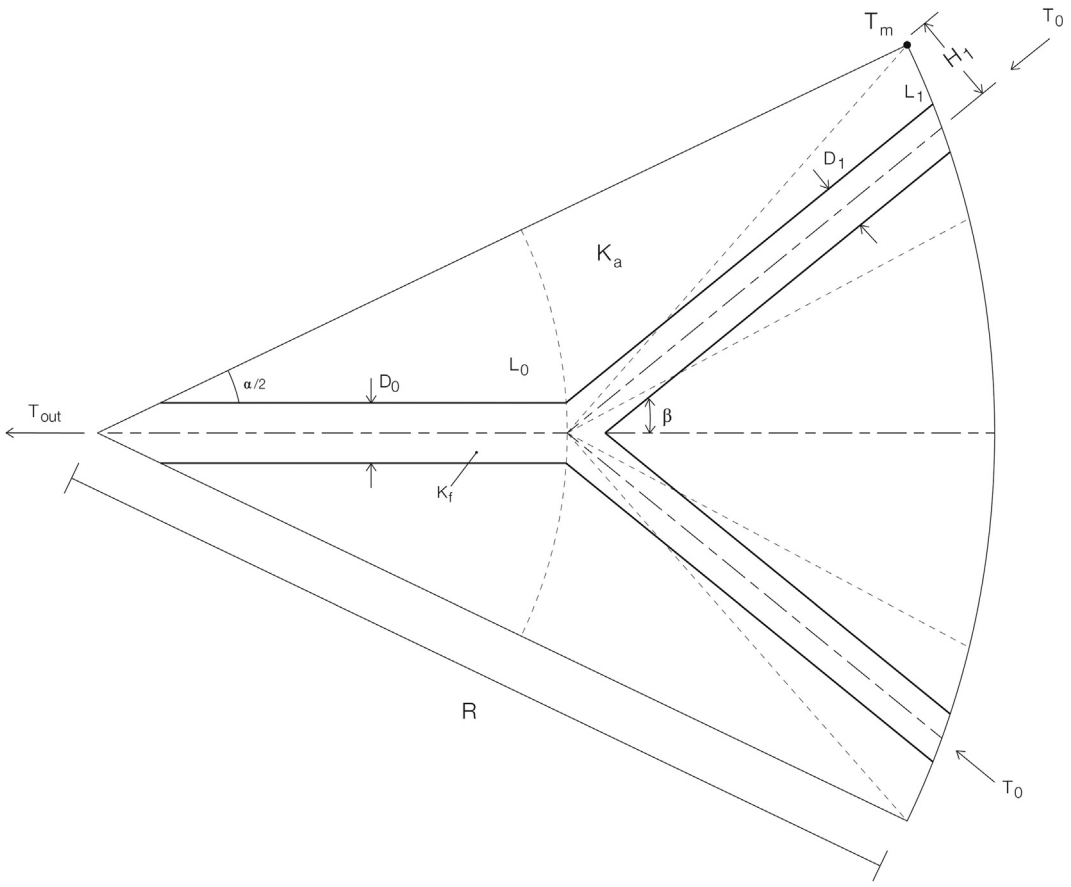

Fig. 2. Second element of construction.

in the same manner as the previous constructal element. The branched network with two levels of ramification can be appreciated in Fig. 3.

The lengths of the pipes array can be defined by the following relations:

$$L_0 = R\left[cos\left(\frac{\alpha}{8}\right) - \frac{\sin\left(\frac{\alpha}{8}\right)}{\tan(\gamma)}\right]\left(cos\left(\frac{\alpha}{4}\right) - \sin\left(\frac{\alpha}{4}\right)tan(\beta)\right), \quad (22)$$

$$L_1 = R\frac{sin\left(\frac{\alpha}{4}\right)}{sin(\beta)}\left(cos\left(\frac{\alpha}{8}\right) - \frac{\sin\left(\frac{\alpha}{8}\right)}{tan(\gamma)}\right), \quad (23)$$

$$L_2 = R\frac{sin\left(\frac{\alpha}{8}\right)}{sin(\gamma)}. \quad (24)$$

From the minimum resistance of the flow of the arrangement of pipes and a volume restriction with consideration of the Hess-Murray law, the angles that have a minimum flow resistance are $\gamma = 38.096^\circ$ and the value of the angle β is the same as that obtained in the second level of ramification. The optimal lengths are considered in the temperature profiles, Nusselt number and thermal resistances, and the aspect ratio of the third construction is obtained.

5. Results

The temperature profiles and the thermal resistance for the nanofluid circulating into the pipe of the first constructal element are shown in Figs. 4 and 5. In the following figures, we use the fixed values of $\dot{q}_0 = 100\ \mathrm{W/m^2}$, $\widehat{H}_0 = 0.01$, $Pe = 100$ and a dimensionless time $\tau = 1.57$. This time corresponds to the maximum amplitude of the solar sinusoidal function. The thermophysical properties of the alumina (Al_2O_3) and base fluid are taken from Büyük Öğüt (2009) and given in Table 1.

In Fig. 4, we show the dimensionless temperature θ_f versus the dimensionless coordinate χ for different values of the volumetric fraction; for $\phi = 0.0$ the base fluid (water) case is obtained. The outlet temperature at $\chi = 1$, for a volumetric fraction of $\phi = 0.04$, presents a higher value. This effect is due to the change in the thermal properties of nanofluid.

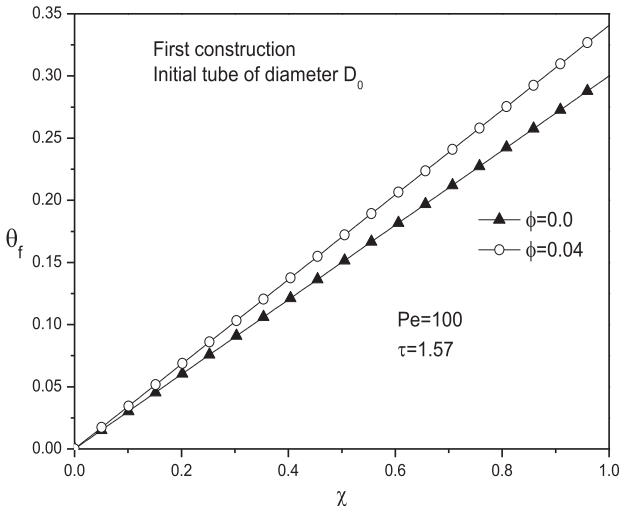

Fig. 4. Temperature profile in the longitudinal direction χ.

From the horizontal and vertical, we define the thermal resistance $\widetilde{T}_0$. It is possible to obtain the value of the aspect ratio $\widehat{H}_0$, given by Eq. (18); in Fig. 5, we can observe that the thermal resistance presents a minimum, $\widehat{H}_0 \cong 0.007$, for values of the volumetric fraction between $\phi = 0.0$ and 0.04. This shows that the geometry of the first constructal element is slender, as required by the constructal theory.

For a volumetric concentration of $\phi = 0.04$, average Nusselt number present lesser values compared with the values of the Nusselt number for a null volumetric concentration. This

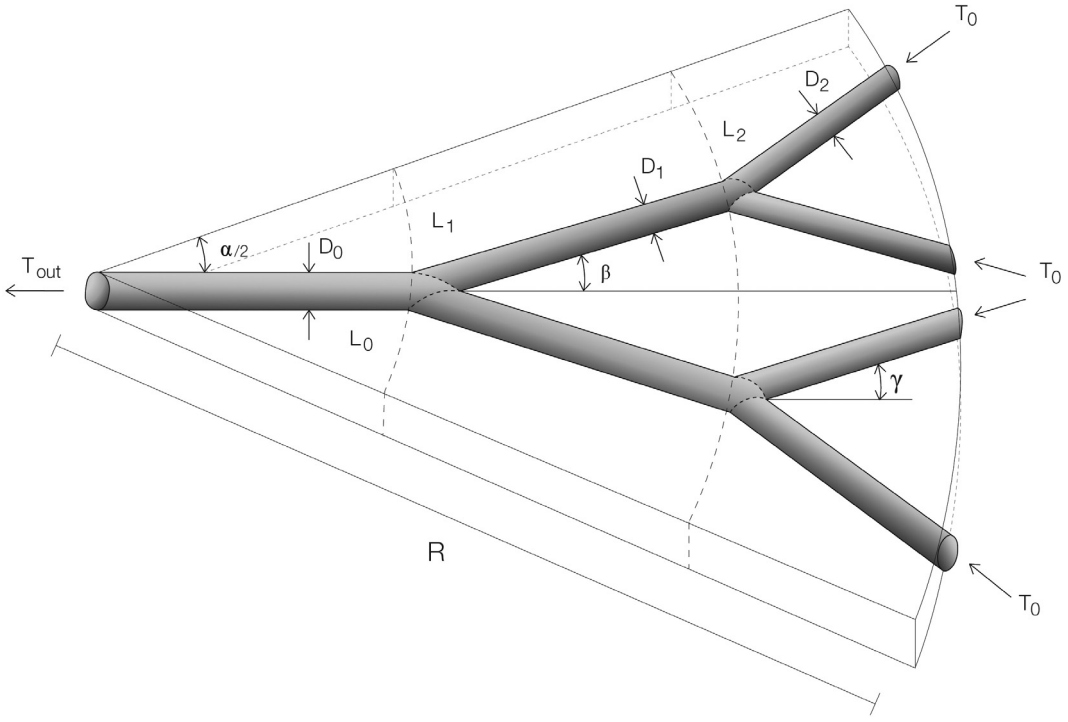

Fig. 3. Ramified network with two levels of ramification.

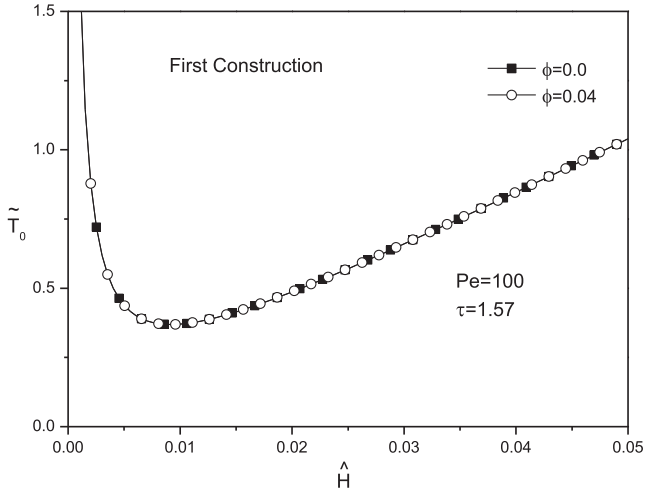

Fig. 5. Thermal resistance versus aspect ratio.

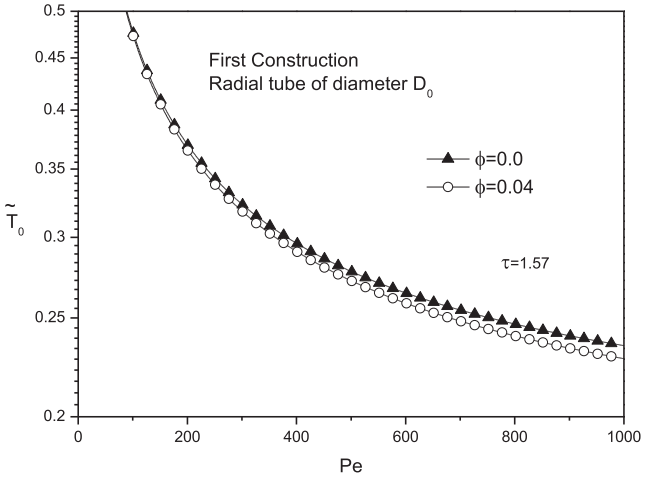

Fig. 7. Thermal resistance of the first constructal element.

Table 1
Thermo-physical properties of base fluid and nanoparticles.

Property	Water	Al_2O_3
ρ [kg/m^3]	997.1	3970
C_P [J/kg K]	4179	765
k [W/m K]	0.613	40

behaviour is interpreted as follows, for a volumetric concentration value of $\phi = 0.04$ the nanofluid thermal conductivity is increased and is greater than fluid base thermal conductivity, a lower average Nusselt number along the pipe in the first construction means that the conductivity heat transfer process is greater than convective process. The dimensionless average Nusselt number for the first construction is shown in Fig. 6.

The thermal resistance of the first constructal element, $\widetilde{T}_0$, tends to decrease as the dimensionless Peclet number, *Pe*, increases, as can be seen in Fig. 7; an increase of the *Pe* means that the velocity in the pipe of diameter D_0 increases. In the same manner as in the calculation of the average Nusselt number, the expression of the aspect ratio $\widehat{H}_0$ is used. The influence of the volumetric fraction of the nanoparticle in the base fluid is reflected with a minor value of the thermal resistance for a value of the volumetric fraction $\phi = 0.04$; thermal resistance is calculated for a time when solar radiation is the highest, according to the sinusoidal model proposed for the incident radiation on the constructal element. It can be established that by modifying the thermal conductivity of the fluid by increasing the volume fraction of the nanoparticles, a lower heat resistance is obtained in comparison with a volume fraction $\phi = 0.0$, corresponding to the thermal conductivity of the base fluid.

In the following figures, the results of the branched network of pipes with two levels of ramification are shown; the dichotomous characteristic of the pipes follows the Hess-Murray law for the flow of nanofluid in the pipes. The increment of the dimensionless temperature θ_f along the dimensionless longitudinal length χ in the different pipes of diameters D_0, D_1 and D_2 for one branch of each level of ramification, is shown in Fig. 8. The temperature profiles present an increment of temperature for every level of ramification; the dimensionless temperature at the outlet of the last construction element is higher than the previous construction for values of the volumetric fraction of $\phi = 0.04$; the dimensionless temperature presents a similar behaviour of the first constructal element and the temperature is higher than the case of volumetric fraction of $\phi = 0.0$.

The geometric configuration of the pipe network covers more area of the semi-circular disc shape body exposing the nanofluid flow in the pipes and increase the heat gains due to the solar

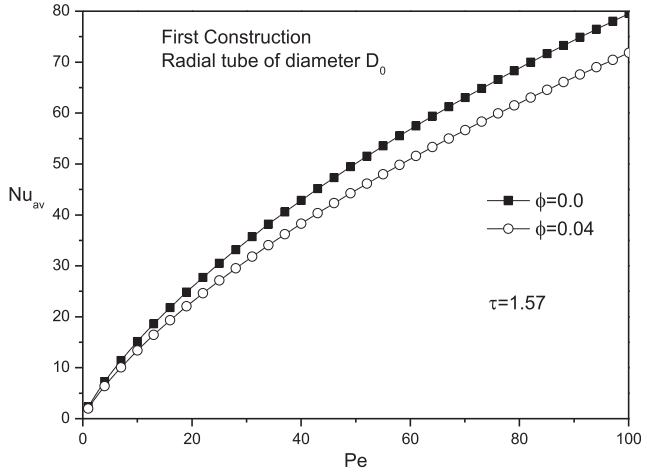

Fig. 6. Nusselt number for the first constructal element.

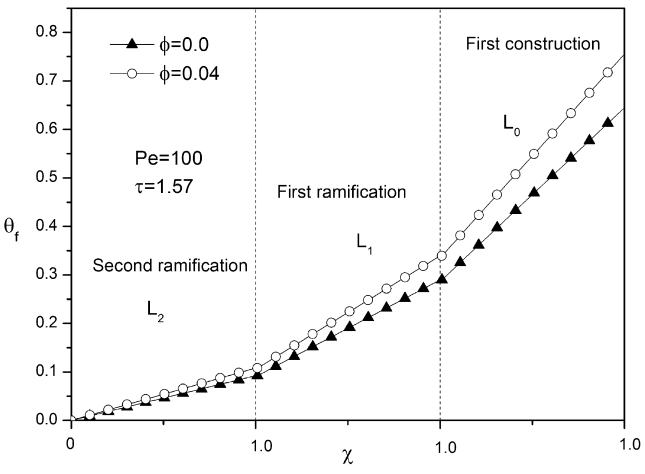

Fig. 8. Longitudinal temperature for different branched levels of the pipe network.

exposition. The lengths defined in Eqs. (21)–(23) are considered in the calculation of the following results.

The aspect ratio of every level of ramification can be calculated, following the methodology applied to the first construction. In Fig. 9 the curves of the thermal resistance $\widetilde{T}_i$ versus aspect ratio $\widehat{H}_i$ for the two volumetric concentrations are shown. For a null volumetric concentration value, correspond to the base fluid, aspect relation values are shown in Fig. 8a, for the first constructal element the aspect ratio is $\widehat{H}_0 \cong 0.07$, for first ramification $\widehat{H}_1 \cong 0.09$ and second ramification $\widehat{H}_2 \cong 0.03$, that corresponding to minimum values of thermal resistance $\widetilde{T}_0 \cong 1.0$, $\widetilde{T}_1 \cong 1.1$ and $\widetilde{T}_2 \cong 0.25$, respectively.

In Fig. 9b corresponding to a volumetric concentration of $\phi = 0.04$, aspect ratio values are similar to the previous case showed in Fig. 9a, for these values thermal resistance shows lower values for every level of ramification. The values of the aspect ratio of every level of ramification are less than unity, considering the definition of $\widehat{H}_i$ as a geometrical parameter in thermal resistance expression, this means that constructal elements composing the branched network are of a slender geometry.

For a volume fraction of $\phi = 0.04$ the constructal elements are smaller than the dimensions of the constructal elements for the base fluid case. This means that for a nanoparticle fraction in a fluid base, the size of the branched network is smaller, and shows a lower thermal resistance than the case of the base fluid, defined by a value of volumetric fraction of $\phi = 0.0$.

The average Nusselt number versus Peclet number for a branched network is shown in Fig. 10. For a nanofluid with volumetric fraction of $\phi = 0.04$ the values of the dimensionless Nusselt number are smaller than the corresponding values for a fluid base case. For the second level of ramification average Nusselt numbers tends to decrease.

The thermal resistance of each level of ramification for both values of volumetric fraction can be seen in Fig. 11. The first construction corresponds to the case of a single pipe of diameter D_0 with a flow of a nanofluid from the periphery to the centre. For a first ramification we consider two pipes of diameter D_1 and a single pipe of diameter D_0. The thermal resistances of the branched pipes can be considered as electrical resistances, in series and in parallel, and the equivalent resistance can be calculated considering the

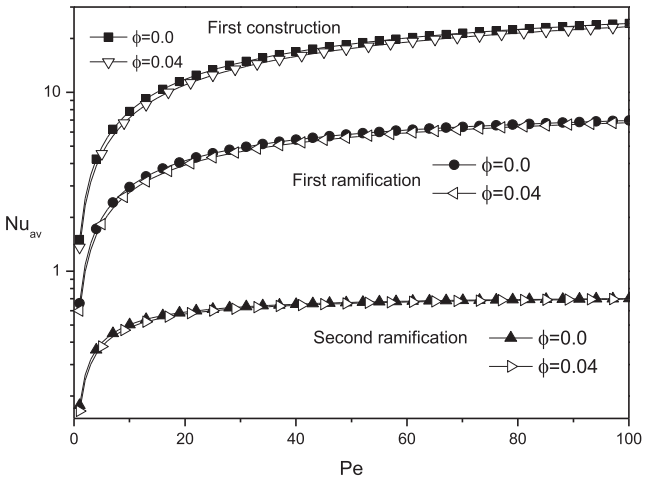

Fig. 10. Average Nusselt number for two levels of ramification.

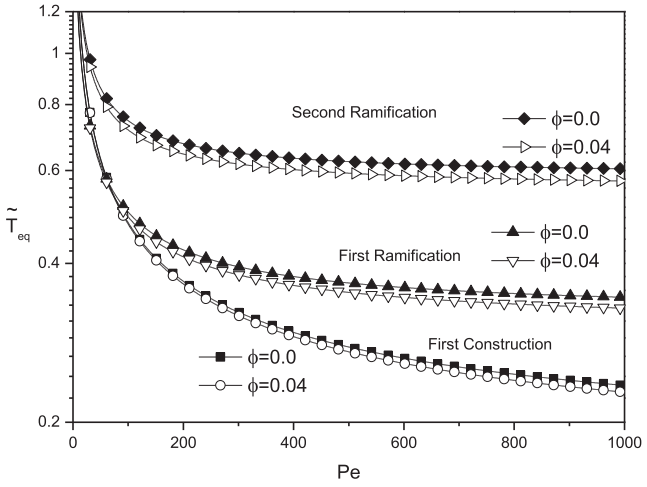

Fig. 11. Equivalent thermal resistance versus Peclet number for different levels of ramifications.

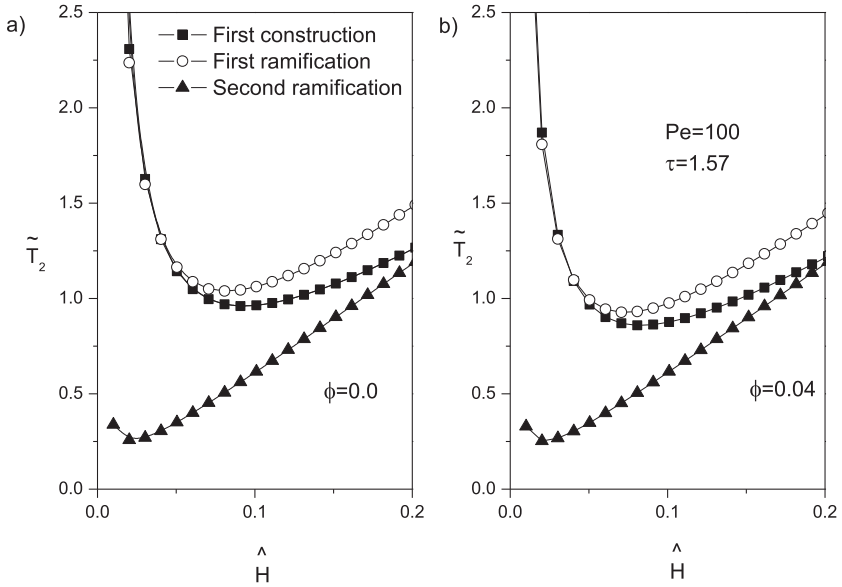

Fig. 9. Aspect ratio versus thermal resistance for values of volumetric fraction (a) $\phi = 0.0$ and (b) $\phi = 0.04$.

electrical analogy (Kou et al., 2009). This procedure is applied for the case of two levels of ramification. In Fig. 11, the equivalent thermal resistances show higher values of the equivalent thermal resistances for two levels of ramification in comparison to a single pipe.

6. Concluding remarks

In the present work, we developed the expressions for a pipe network in a solar collector with a nanofluid as a work fluid. For volumetric concentrations of 0.04, the size of the constructal elements are smaller in comparison to a volumetric fraction equal to zero; this allows for the design of smaller networks. The methodology proposed by the constructal theory is a tool for designing networks in function of the physical and geometrical elements, which cover a large area in a given volume. The heat gained by the nanofluid can be transmitted through heat exchangers for later use.

Network modelling of dendritic geometry by the constructal theory presents a challenge, with the problem of determining an optimal point where the hydraulic and thermal resistances are minimal, and considering the characteristics of the nanofluid as the factor of friction or viscosity.

Acknowledgements

This work has been supported by a research grant No. 258849 CB-CONACYT 2015 of Consejo Nacional de Ciencia y Tecnología at Mexico.

References

Abbasi, F.M., Hayat, T., Ahmad, B., 2015. Peristalsis of silver-water nanofluid in the presence of Hall and Ohmic heating effects: applications in drug delivery. J. Mol. Liq. 207, 248–255. http://dx.doi.org/10.1016/j.molliq.2015.03.042.

Angayarkanni, S.A., Philip, J., 2015. Review on thermal properties of nanofluids: recent developments. Adv. Coll. Interf. Sci. 225, 146–176. http://dx.doi.org/10.1016/j.cis.2015.08.014.

Bai, C., Wang, L., 2013. Two nanofluid configurations for heat conductions systems: performance comparison. Int. J. Heat Mas Transf. 66, 632–641. http://dx.doi.org/10.1016/j.ijheatmasstransfer.2013.07.040.

Bai, C., Wang, L., 2011. Constructal blade shape in nanofluids. Nanoscale Res. Lett. 6, 240. http://dx.doi.org/10.1186/1556-276X-6-240.

Bejan, A., 2013. Convection Heat Transfer. Wiley and Sons, New Jersey.

Bejan, A., 2000. Shape and Structure, From Engineering to Nature. Cambridge University Press, Cambridge.

Buongiorno, J., 2006. Convective transport in nanofluids. J. Heat Transf. 128, 240–250. http://dx.doi.org/10.1115/1.2150834.

Buongiorno, J., Venerus, D.C., Prabhat, N., McKrell, T., Townsend, J., Christianson, R., Tolmachev, Y.V., Keblinski, P., Hu, L., Alvarado, J.L., Bang, I.C., Bishnoi, S.W., Bonetti, M., Botz Botz, F., Cecere, A., Chang, Y., Chen, G., Chen, H., Chung, S.J., Chyu, M.K., Das, S.K., Di Paola, R., Ding, Y., Dubois, F., Dzido, G., Eapen, J., Escher, W., Funfschilling, D., Galand, Q., Gao, J., Gharagozloo, P.E., Goodson, K.E., Gutierrez, J.G., Hong, H., Horton, M., Hwang, K.S., Iorio, C.S., Jang, S.P., Jarzebski, A.B., Jiang, Y., Jin, L., Kabelac, S., Kamath, A., Kedzierski, M.A., Kieng, L.G., Kim, C., Kim, J.-H., Kim, S., Lee, S.H., Leong, K.C., Manna, I., Michel, B., Ni, R., Patel, H.E., Philip, J., Poulikakos, D., Reynaud, C., Savino, R., Singh, P.K., Song, P., Sundararajan, T., Timofeeva, E., Tritcak, T., Turanov, A.N., Van Vaerenbergh, S., Wen, D., Witharana, S., Yang, C., Yeh, W.-H., Zhao, X.-Z., Zhou, S.-Q., 2009. A benchmark study on the thermal conductivity of nanofluids. J. Appl. Phys. 106, 94312. http://dx.doi.org/10.1063/1.3245330.

Büyük Öğüt, E., 2009. Natural convection of water-based nanofluids in an inclined enclosure with a heat source. Int. J. Therm. Sci. 48, 2063–2073. http://dx.doi.org/10.1016/j.ijthermalsci.2009.03.014.

Chen, C.-H., Ding, C.-Y., 2011. Study on the thermal behavior and cooling performance of a nanofluid-cooled microchannel heat sink. Int. J. Therm. Sci. 50, 378–384. http://dx.doi.org/10.1016/j.ijthermalsci.2010.04.

Daungthongsuk, W., Wongwises, S., 2007. A critical review of convective heat transfer of nanofluids. Renew. Sustain. Energy Rev. 11, 797–817. http://dx.doi.org/10.1016/j.rser.2005.06.005.

Drew, D.A., Passman, S.L., 1999. Theory of Multicomponent Fluids. Springer, New York.

Fan, J., Wang, L., 2010. Constructal design of nanofluids. Int. J. Heat Mass Transf. 53, 4238–4247. http://dx.doi.org/10.1016/j.ijheatmasstransfer.2010.05.050.

Ghanbarpour, M., Bitaraf Haghigi, E., Khodabandeh, R., 2014. Thermal properties and rheological behavior of water based Al_2O_3 nanofluid as a heat transfer fluid. Exp. Therm. Fluid Sci. 53, 227–235. http://dx.doi.org/10.1016/j.expthermflusci.2013.12.013.

Godson, L., Raja, B., Mohan Lal, D., Wongwises, S., 2010. Enhancement of heat transfer using nanofluids – an overview. Renew. Sustain. Energy Rev. 14, 629–641. http://dx.doi.org/10.1016/j.rser.2009.10.004.

Hamilton, R.L., Crosser, O.K., 1962. Thermal conductivity of heterogeneous two-component systems. Indian Eng. Chem. Fund. 1, 187–191.

Hatami, M., Domairry, G., Mirzababaei, S.N., 2017. Experimental investigation of preparing and using the H_2O based nanofluids in the heating process of HVAC system model. Int. J. Hydrogen Energy 6–11. http://dx.doi.org/10.1016/j.ijhydene.2016.12.104.

Kalogirou, S.A., 2004. Solar thermal collectors and applications. Prog. Energy Combust. Sci. 30, 231–295. http://dx.doi.org/10.1016/j.pecs.2004.02.001.

Keblinski, P., Eastman, J.A., Cahill, D.G., 2005. Nanofluids for thermal transport. Mater. Today 8, 36–44. http://dx.doi.org/10.1016/S1369-7021(05)70936-6.

Keblinski, P., Phillpot, S.R., Choi, S.U.S., Eastman, J.A., 2002. Mechanisms of heat flow in suspensions of nano-sized particles (nanofluids). Int. J. Heat Mass Transf. 45, 855–863. http://dx.doi.org/10.1016/S0017-9310(01)00175-2.

Khaleduzzaman, S.S., Sohel, M.R., Saidur, R., Mahbubul, I.M., Shahrul, I.M., Akash, B. A., Selvaraj, J., 2014. Energy and exergy analysis of alumina-water nanofluid for an electronic liquid cooling system. Int. Commun. Heat Mass Transf. 57, 118–127. http://dx.doi.org/10.1016/j.icheatmasstransfer.2014.07.015.

Kleinstreuer, C., Li, J., Koo, J., 2008. Microfluidics of nano-drug delivery. Int. J. Heat Mass Transf. 51, 5590–5597. http://dx.doi.org/10.1016/j.ijheatmasstransfer.2008.04.043.

Koo, J., Kleinstreuer, C., 2005. Laminar nanofluid flow in microheat-sinks. Int. J. Heat Mass Transf. 48, 2652–2661. http://dx.doi.org/10.1016/j.ijheatmasstransfer.2005.01.029.

Kou, J.-L., Hang-Jun, L., Feng-Min, W., You-Sheng, X., 2009. Analysis of thermal conductivity in tree-like branched networks. Chin. Phys. B 18 (4), 1553–1559.

Liu, Z.H., Hu, R.L., Lu, L., Zhao, F., Xiao, H.S., 2013. Thermal performance of an open thermosyphon using nanofluid for evacuated tubular high temperature air solar collector. Energy Convers. Manag. 73, 135–143. http://dx.doi.org/10.1016/j.enconman.2013.04.010.

Lu, L., Liu, Z.H., Xiao, H.S., 2011. Thermal performance of an open thermosyphon using nanofluids for high-temperature evacuated tubular solar collectors. Part 1: Indoor experiment. Sol. Energy 85, 379–387. http://dx.doi.org/10.1016/j.solener.2010.11.008.

Miguel, A.F., 2015. Fluid flow in a porous tree-shaped network: optimal design and extension of Hess-Murray's law. Physica A 423, 61–71. http://dx.doi.org/10.1016/j.physa.2014.12.025.

Nasrin, R., Alim, M.A., 2014. Semi-empirical relation for forced convective analysis through a solar collector. Sol. Energy 105, 455–467. http://dx.doi.org/10.1016/j.solener.2014.03.035.

Puliti, G., Paolucci, S., Sen, M., 2012. Nanofluids and their properties. ASME. Appl. Mech. Rev. 64 (3). http://dx.doi.org/10.1115/1.4005492. 030803-1–030803-23.

Putra, N., Roetzel, W., Das, S.K., 2003. Natural convection of nano-fluids. Heat Mass Transf. 39, 775–784. http://dx.doi.org/10.1007/s00231-002-0382-z.

Sarsam, W.S., Kazi, S.N., Badarudin, A., 2015. A review of studies on using nanofluids in flat-plate solar collectors. Sol. Energy 122, 1245–1265. http://dx.doi.org/10.1016/j.solener.2015.10.032.

Sözen, A., Özbaş, E., Menlik, T., Çakir, M.T., Gürü, M., Boran, K., 2014. Improving the thermal performance of diffusion absorption refrigeration system with alumina nanofluids: an experimental study. Int. J. Refrig. 44, 73–80. http://dx.doi.org/10.1016/j.ijrefrig.2014.04.018.

Taylor, R.A., Otanicar, T., Rosengarten, G., 2012. Nanofluid-based optical filter optimization for PV/T systems. Light Sci. Appl. 1, 1–7. http://dx.doi.org/10.1038/lsa.2012.34.

Wechsatol, W., Lorente, S., Bejan, A., 2002. Optimal tree-shaped networks for fluid flow in a disc-shaped body. Int. J. Heat Mass Transf. 45, 4911–4924. http://dx.doi.org/10.1016/S0017-9310(02)00211-9.